BJ www.biochemj.org

BJ Structure

Biochem. J. (2010) **432**, 445–450 (Printed in Great Britain) doi:10.1042/BJ20101241

online data

Structural insights into the catalytic mechanism of the yeast pyridoxal 5-phosphate synthase Snz1

Xuan ZHANG, Yan-Bin TENG, Jian-Ping LIU, Yong-Xing HE, Kang ZHOU, Yuxing CHEN and Cong-Zhao ZHOU[1]

Hefei National Laboratory for Physical Sciences at Microscale and School of Life Sciences, University of Science and Technology of China, Hefei, Anhui 230027, People's Republic of China

In most eubacteria, fungi, apicomplexa, plants and some metazoans, the active form of vitamin B6, PLP (pyridoxal 5-phosphate), is *de novo* synthesized from three substrates, R5P (ribose 5-phosphate), DHAP (dihydroxyacetone phosphate) and ammonia hydrolysed from glutamine by a complexed glutaminase. Of the three active sites of DXP (deoxyxylulose 5-phosphate)-independent PLP synthase (Pdx1), the R5P isomerization site has been assigned, but the sites for DHAP isomerization and PLP formation remain unknown. In the present study, we present the crystal structures of yeast Pdx1/Snz1, in apo-, G3P (glyceraldehyde 3-phosphate)- and PLP-bound forms, at 2.3, 1.8 and 2.2 Å (1 Å = 0.1 nm) respectively. Structural and biochemical analysis enabled us to assign the PLP-formation site, a G3P-binding site and a G3P-transfer site. We propose a putative catalytic mechanism for Pdx1/Snz1 in which R5P and DHAP are isomerized at two distinct sites and transferred along well-defined routes to a final destination for PLP synthesis.

Key words: catalytic mechanism, crystal structure, isomerization, pyridoxal 5-phosphate synthase, *Saccharomyces cerevisiae*, site-directed mutagenesis.

INTRODUCTION

The active form of vitamin B6, PLP (pyridoxal 5-phosphate), is an essential cofactor for numerous metabolic enzymes. PLP also has an important role in amino acid and carbohydrate metabolism [1,2]. To date, two pathways for the *de novo* biosynthesis of PLP have been characterized that differ in their dependence on DXP (deoxyxylulose 5-phosphate). The DXP-dependent pathway is found in a small number of eubacteria that synthesize PLP from DXP and 4-phosphohydroxy-L-threonine. This reaction is catalysed by enzymes in the Pdx family (Pdx A, B, C, F, H, J and GapA) [3] (Scheme 1). In contrast, the DXP-independent pathway is predominantly found in most eubacteria, fungi, apicomplexa, plants and some metazoans. The pathway reactions are catalysed by a complex of two proteins, Pdx1 (PLP synthase) and Pdx2 (glutaminase) [4]. This pathway uses three substrates: R5P (ribose 5-phosphate) or its isomer RBP (ribulose 5-phosphate), DHAP (dihydroxyacetone phosphate) or its isomer G3P (glyceraldehyde 3-phosphate) and ammonia, which is hydrolysed from glutamine (Scheme 1).

Compared with the extensively studied DXP-dependent pathway in *Escherichia coli*, the structural basis for the DXP-independent pathway is poorly understood, despite the availability of structural data on several Pdx1 enzymes. The crystal structure of *Geobacillus stearothermophilus* Pdx1 (*Gs*Pdx1) is a dodecamer of two stacked hexameric rings, with each monomer adopting a classic $(\beta/\alpha)_8$ fold [5]. Crystal structures of Pdx1 from *Bacillus subtilis* and *Thermotoga maritima* (*Bs*Pdx1 and *Tm*Pdx1 respectively) in complex with the corresponding glutaminase revealed a four-layered sandwich assembly of 24 subunits, adopting a double-layered core of dodecameric Pdx1, with a hexameric ring of glutaminase attached on each side [6,7]. In the presence of ammonia, *Bs*Pdx1 alone catalyses a series of reactions to produce PLP, including isomerization of the pentose and triose, imine formation, ammonia addition and aromatic ring formation. Lys^{149} of *Bs*Pdx1 was found to be involved in adduct formation with RBP using Fourier-transform ion-cyclotron resonance MS with electrospray ionization capabilities [8], whereas the crystal structure of *Tm*Pdx1 showed that the pentulose phosphate imine was adducted to Lys^{82} (Lys^{81} of *Bs*Pdx1) [7]. Enzymatic assays indicated that *Bs*Pdx1 K81A and K149A mutants lost the ability to catalyse PLP synthesis. The K81A mutant lacked R5P-to-RBP isomerization activity, whereas the K149A mutant catalysed the isomerization at a faster velocity than the wild-type. These results demonstrated that both Lys^{81} and Lys^{149} of *Bs*Pdx1 are essential for PLP formation, but only Lys^{81}, and not Lys^{149}, catalyses the R5P to RBP isomerization. However, the DHAP-isomerization site and the final PLP-formation site remain unknown.

Bacterial Pdx1 homologues are reported to exist in a hexamer/dodecamer equilibrium [5,6], but a 3.0 Å (1 Å = 0.1 nm) crystal structure of the *Saccharomyces cerevisiae* PLP synthase Pdx1/Snz1 shows that it exists as a hexamer, both in the crystal and in solution [9]. The yeast genome harbours three *PDX1* paralogues, named *SNZ1*, *SNZ2* and *SNZ3*, each of which is flanked by a *PDX2* gene of *SNO1*, *SNO2* or *SNO3* at the complementary chain [10]. The gene pairs *SNZ2*/*SNO2* and *SNZ3*/*SNO3* are involved in thiamine synthesis, whereas *SNZ1*/*SNO1* is essential for *de novo* PLP biosynthesis [11]. In the present study we report three crystal structures for Snz1 in apo-, G3P-bound and PLP-bound forms, at 2.3, 1.8 and 2.2 Å respectively. Using activity assays and site-directed mutagenesis, we assigned the PLP-formation site and two irreversible transfer routes of RBP and G3P.

Abbreviations used: DHAP, dihydroxyacetone phosphate; DXP, deoxyxylulose 5-phosphate; G3P, glyceraldehyde 3-phosphate; H-bond, hydrogen bond; Pdx1, pyridoxal 5-phosphate synthase; *Bs*Pdx1, *Bacillus subtilis* Pdx1; *Gs*Pdx1, *Geobacillus stearothermophilus* Pdx1; *Tm*Pdx1, *Thermotoga maritima* Pdx1; PLP, pyridoxal 5-phosphate; RBP, ribulose 5-phosphate; RMSD, root mean square deviation; R5P, ribose 5-phosphate; TIM, triosephosphate isomerase.

[1] To whom correspondence should be addressed (email zcz@ustc.edu.cn).

Atomic co-ordinates and structure factors were deposited in the PDB (http://www.rcsb.org) under accession codes 3O05, 3O06 and 3O07.

Table 1 Crystal parameters, data collection and structure refinement

For the resolution range, the values in parentheses refer to statistics in the highest bin. $R_{merge} = \Sigma_{hkl} \Sigma_i |I_i(hkl) - \langle I(hkl) \rangle| / \Sigma_{hkl} \Sigma_i I_i(hkl)$, where $I_i(hkl)$ is the intensity of an observation and $\langle I(hkl) \rangle$ is the mean value for its unique reflection; summations are over all reflections. R-factor $= \Sigma_h |F_o(h) - F_c(h)| / \Sigma_h F_o(h)$, where F_o and F_c are the observed and calculated structure–factor amplitudes respectively. R-free was calculated with 5 % of the data excluded from the refinement. RMSDs are from ideal values.

Data collection	Apo-form	Snz1–G3P	Snz1–PLP
Space group	$P22_12_1$	$P22_12_1$	$P22_12_1$
Unit cell (Å, °)	a = 59.31, b = 110.38, c = 156.39, $\alpha = \beta = \gamma = 90.00$	a = 60.47, b = 111.97, c = 158.74, $\alpha = \beta = \gamma = 90.00$	a = 58.97, b = 109.42, c = 155.39, $\alpha = \beta = \gamma = 90.00$
Molecules per asymmetric unit	3	3	3
Resolution range (Å)	110.38–2.35 (2.41–2.35)	50.00–1.80 (1.83–1.80)	32.44–2.20 (2.24–2.20)
Unique reflections	43496 (765)	95196 (5006)	51330 (2622)
Completeness (%)	92.7 (91.4)	99.5 (99.4)	99.2 (97.4)
$\langle I/\sigma(I) \rangle$	14.4 (1.7)	29.1 (1.6)	13.5 (3.2)
R_{merge} (%)	8.3 (32.9)	7.8 (22.0)	9.8 (60.1)
Average redundancy	4.9 (3.5)	5.8 (5.6)	4.5 (3.8)
Structure refinement			
Resolution range (Å)	110.38–2.35	158.74–1.80	32.44–2.20
R-factor/R-free (%)	20.41/25.13	20.34/23.58	19.40/22.74
Number of protein atoms	5798	6046	5871
Number of water atoms	76	753	348
RMSD bond lengths (Å)	0.022	0.012	0.009
RMSD bond angles (°)	1.844	1.167	1.095
Mean B factors (Å^2)	22.17	22.53	22.15
Ramachandran plot*			
Most favoured (%)	95.83	98.38	97.67
Additional allowed (%)	3.65	1.62	2.33
Outliers (%)	0.52	0	0
PDB code	3O06	3O07	3O05

*Categories were defined by MolProbity

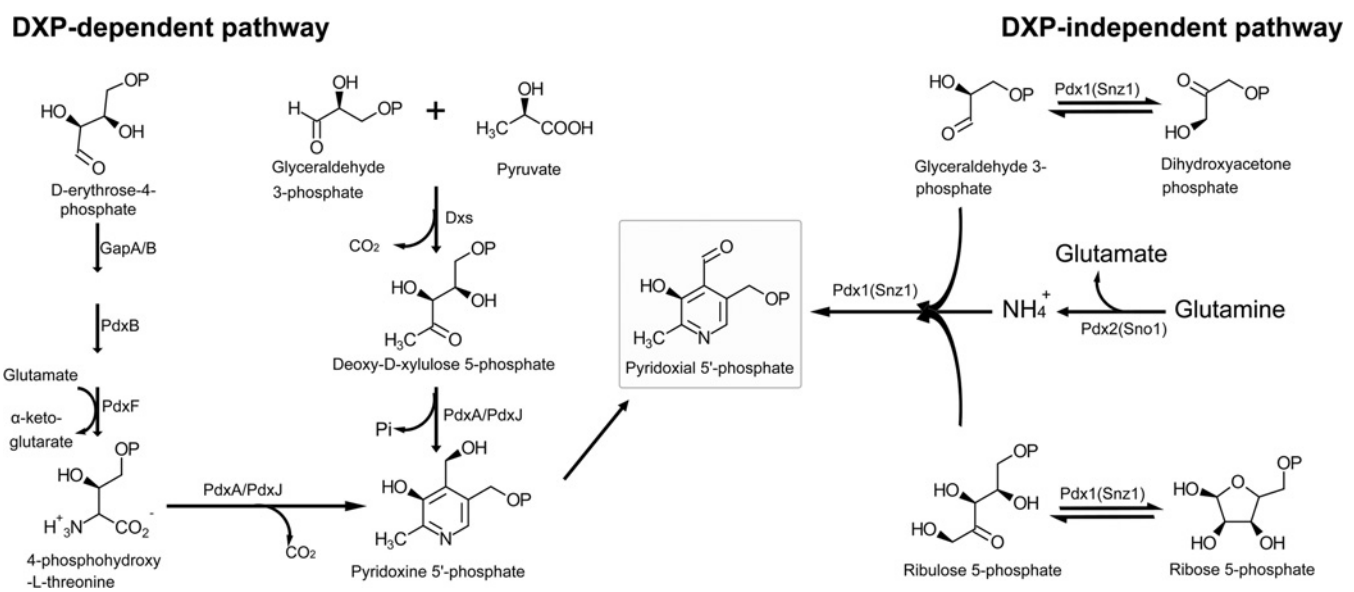

Scheme 1 Two different pathways for the *de novo* biosynthesis of PLP

EXPERIMENTAL

Crystallization and structure determination

Wild-type and mutant Snz1 were overexpressed in *E. coli* and purified with Ni-NTA (Ni^{2+}-nitrilotriacetate) affinity chromatography followed by gel filtration. Crystals of the apo- and ligand-bound Snz1 were grown by hanging-drop vapour diffusion at 16 °C. The datasets of apo- and ligand-bound Snz1 were collected at the Shanghai Synchrotron Radiation Facility, using beamline BL17U ($\lambda = 0.9795$ Å) at 100 K with a MX-225 CCD (Marresearch, Germany). All structures were determined by molecular replacement using the *Gs*Pdx1 structure (PDB code 1ZNN) [5] with Phaser [12] in CCP4 [13]. Refinement was carried out using REFMAC [14] and Coot [15]. The overall assessment of model quality was performed using MolProbity [16]. Atomic co-ordinates and structure factors were deposited in the PDB (http://www.rcsb.org) under accession codes 3O05, 3O06 and 3O07. Crystallographic parameters are listed in Table 1. All structure Figures were prepared with PyMOL (DeLano Scientific; http://www.pymol.org). Further details can be

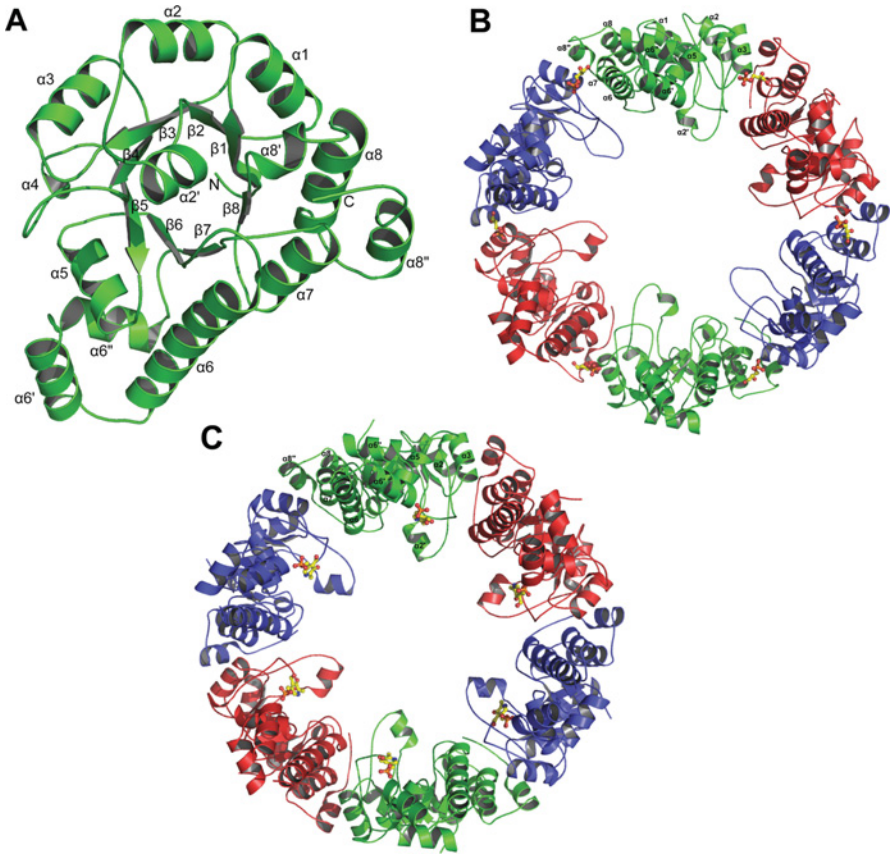

Figure 1 Overall structure of Snz1

(**A**) A monomer of Snz1; α-helices and β-strands are labelled sequentially. The hexameric ring of (**B**) Snz1–G3P and (**C**) Snz1–PLP. Monomers are alternatively coloured in blue, green and red. G3P and PLP molecules are shown as sticks.

found in the Supplementary material at http://www.BiochemJ.org/bj/432/bj4320445add.htm.

Enzymatic assays

PLP formation activity assays were performed as described previously [17]. Briefly, in a 200 μl reaction mix containing 20 μM Snz1 or mutants, 2 mM R5P, 2 mM DHAP and 10 mM ammonium sulfate in 50 mM Tris/HCl (pH 8.0), PLP absorbance at 414 nm was monitored. Measurements were set to occur at 5-min intervals for a total of 80 min, using a DU800 spectrophotometer (Beckman Coulter) equipped with a cuvette holder fixed at 37 °C.

DHAP isomerization

Either 10 mM DHAP or G3P was incubated with 40 μM Snz1 or mutants in 50 mM phosphate buffer (pH 8.0) in ^2H_2O at 30 °C for 4 h. Isomerization reactions in 500 μl were monitored by 500 MHz NMR spectroscopy [18,19]. DHAP and G3P without Snz1 were used as negative controls.

RESULTS AND DISCUSSION

Overall structure

The structure of *Bs*Pdx1 [6] suggested that the N-terminal 14 residues appear to be disordered in the autonomous Snz1 and adopt a defined secondary structure upon binding to Sno1. This region makes no contribution to the *in vitro* Pdx1 activity, as shown by comparisons between the truncated version and the full-length protein (Supplementary Figure S1 at http://www.BiochemJ.org/bj/432/bj4320445add.htm). Therefore we deleted this region for crystal optimization and determined the structure of the apo-form at 2.3 Å. Crystals of G3P-bound (Snz1–G3P) and PLP-bound (Snz1–PLP) forms were obtained by co-crystallization of the apo-form with 10 mM DHAP or 2.5 mM PLP respectively.

The overall structure of the Snz1 monomer has a classic PdxS-fold [5] consisting of eight parallel β-strands, β1–β8, surrounded by eight α-helices, α1–α8, and five insertions, α2', α6', α6", α8' and α8" (Figure 1A). Similar to the structure of *Gs*Pdx1, six monomers formed a hexameric ring (Figure 1B). Superposition of Snz1–PLP and Snz1–G3P over the apo-form gave RMSDs (root mean square deviations) of 0.3 Å and 0.6 Å respectively, for 258 Cα atoms, suggesting that Snz1 undergoes slight conformational changes upon G3P or PLP binding. In Snz1–G3P, a G3P molecule was located at the interface of two adjacent monomers (Figure 1B). The electron density matches G3P very well when contoured at 1.5 σ, and the phosphate group has a density typical of a trilobed head (Supplementary Figure S2A at http://www.BiochemJ.org/bj/432/bj4320445add.htm). At the inner surface of the hexameric ring, each Snz1–PLP monomer harbours a PLP molecule (Figure 1C) that could be well fitted in the electron density map at 1.5 σ (Supplementary Figure S2B).

Similar to the structure of *Gs*Pdx1 [5], Snz1 monomers in the hexameric ring also show extensive hydrophobic contacts.

The interface, composed of helices α7, α8" and the N-terminal moiety of α6 from one monomer and α3 from the neighbouring monomer, buries a total area of approx. 1800 Å^2. Residues Arg^{82}, His^{85}, Asp^{110}, Arg^{164} and Asp^{220} at the interface are highly conserved among Pdx1s from different organisms (Supplementary Figure S3 at http://www.BiochemJ.org/bj/432/bj4320445add.htm). This highly conserved interface of more than 1500 Å^2 makes hexamerization of Pdx1 essential for its multiple activities.

G3P-binding site

The Snz1 used for crystallization catalysed the irreversible isomerization of DHAP to G3P (Supplementary Figure S4 at http://www.BiochemJ.org/bj/432/bj4320445add.htm), so the electron density in the model of Snz1 co-crystallized with DHAP should represent G3P rather than DHAP (Supplementary Figure S2A). The G3P molecule was stabilized at the interface of two monomers by a number of H-bonds (hydrogen bonds) to the G3P oxygen atoms O1P–O4P (Figure 2A). The position of the G3P phosphate group is well defined by H-bonds of O1P-Arg164'Nη1, O1P-Arg164'Nη2, O2P-Wat309, O2P-Arg164'Nη2, O3P-Wat361 and O4P-Glu116Oε1. The involved residues, Gly^{84}, Asp^{110}, His^{114}, Glu^{116} and Arg^{164} are highly conserved (Supplementary Figure S3). This site also undergoes a very slight conformational change upon G3P binding, which is consistent with the relatively high K_m of 0.30 mM and low k_{cat} of 0.02 min^{-1} of Snz1 towards G3P [9]. This indicated that the substrate G3P most likely binds to Snz1 weakly and that the binding mechanism does not involve an induced fit.

The G3P phosphate group is stabilized by three H-bonds to Arg$^{164'}$ and one to Glu^{116} (Figure 2A). The PLP-synthesis activity assays indicated that the R164A mutant is completely inactive, whereas the E116A mutant has the same activity as the wild-type (Supplementary Figure S1). These results demonstrate that the highly conserved Arg^{164} is indispensable for PLP synthesis, whereas the H-bond between Glu^{116} and G3P might be the result of crystal packing.

PLP-binding site

In a shallow cleft on the surface of Snz1–PLP, we found an area of electron density with a trilobed head, reminiscent of a PLP molecule (Supplementary Figure S2B). The four oxygen atoms (O1P–O4P) of the phosphate group form an intensive H-bond network with residues Arg^{136} and Arg^{137}, and four water molecules (Figure 2B). O1P is fixed by Wat354 and Wat371, and O2P by Wat373 and Wat379. O3P forms three H-bonds with Arg136Nε, Arg136Nη2 and Arg137Nη2, whereas O4P forms a single H-bond with Arg137Nη2. O4A and the nitrogen atom of the pyrimidine moiety of PLP form two H-bonds each with Trp111O and Lys148Nε.

In contrast with the PLP molecule binding to Snz1, a phosphate molecule is observed in the structures of both *Tm*Pdx1 and *Gs*Pdx1 [5,7]. Superposition of the phosphate-binding site of *Tm*Pdx1 over the PLP-binding site of Snz1 revealed that the highly conserved residues (Arg^{136} and Arg^{137} in Snz1, Arg^{138} and Arg^{139} in *Tm*Pdx1) share the same H-bonding pattern to the phosphate (Supplementary Figure S5 at http://www.BiochemJ.org/bj/432/bj4320445add.htm). This site has been assigned as binding the phosphate group of DHAP/G3P or the final product PLP [7]. Neither the single-mutant K148A nor the double-mutant R136A/R137A synthesizes PLP (Supplementary Figure S1). Thus we propose that the PLP-binding site in our structure is also the

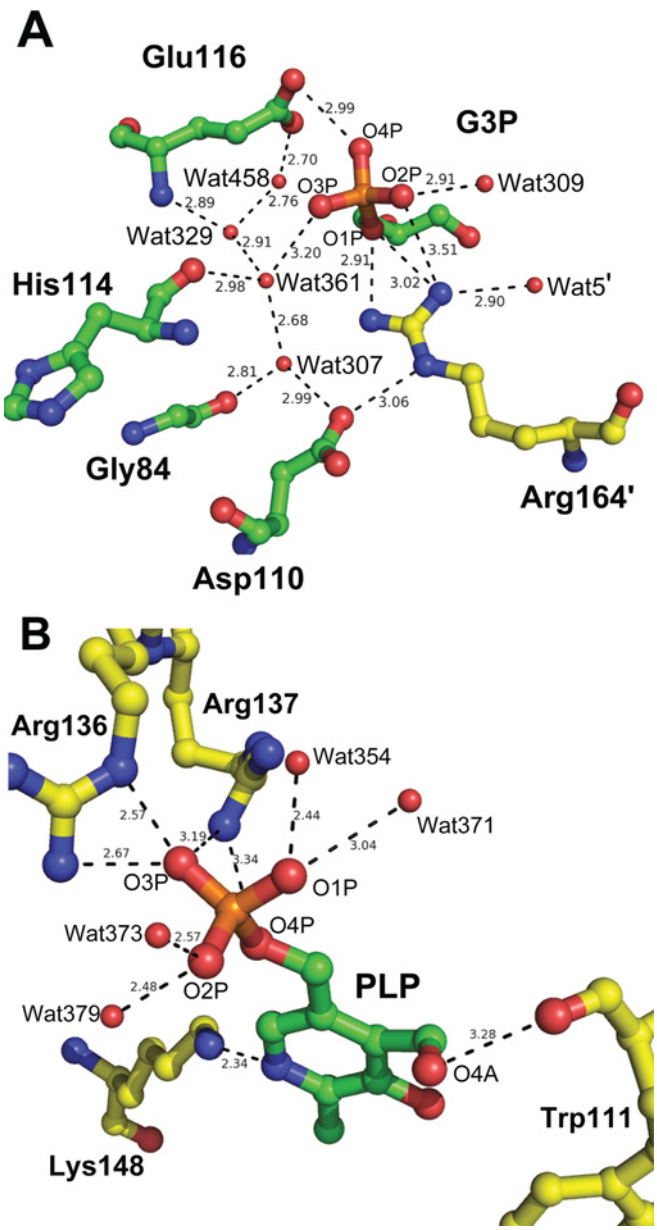

Figure 2 G3P- and PLP-binding sites

(**A**) G3P-binding site. Arg^{164} from the adjacent monomer is marked with a prime. (**B**) PLP-binding site. Oxygen atoms of G3P and PLP are numbered according to PDB files. Bond lengths are labelled in Å.

PLP-formation site, and should also be the final destination of the substrates G3P and RBP.

A distinct mechanism of DHAP isomerization?

Comparative structure analysis of Snz1 using the DALI server (http://www2.ebi.ac.uk/dali/) [20] enabled us to find a TIM (triosephosphate isomerase; EC 5.3.1.1) from *Trypanosoma brucei* in complex with G3P (6TIM) [21] which also belongs to the $(\beta/\alpha)_8$-barrel enzyme family, but catalyses the reversible interconversion of DHAP and G3P through a simple proton transfer [22]. Snz1 has four highly conserved lysine residues Lys^{80}, Lys^{117}, Lys^{148} and Lys^{240} (Supplementary Figure S3), which might be essential for TIM activity [23,24]. Lys^{81} of *Bs*Pdx1 (Lys^{80}

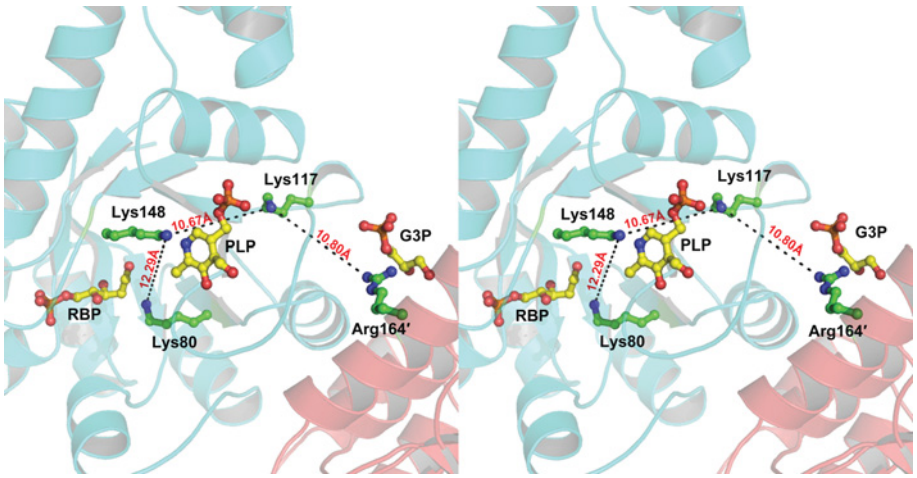

Figure 3 Relative locations of PLP, RBP and G3P

Two monomers of Snz1 are coloured in cyan and red. Side chains of Lys^{80}, Lys^{117}, Lys^{148} and Arg$^{164'}$ from the adjacent monomer are shown as sticks. The distances of H-bonds are shown in Å.

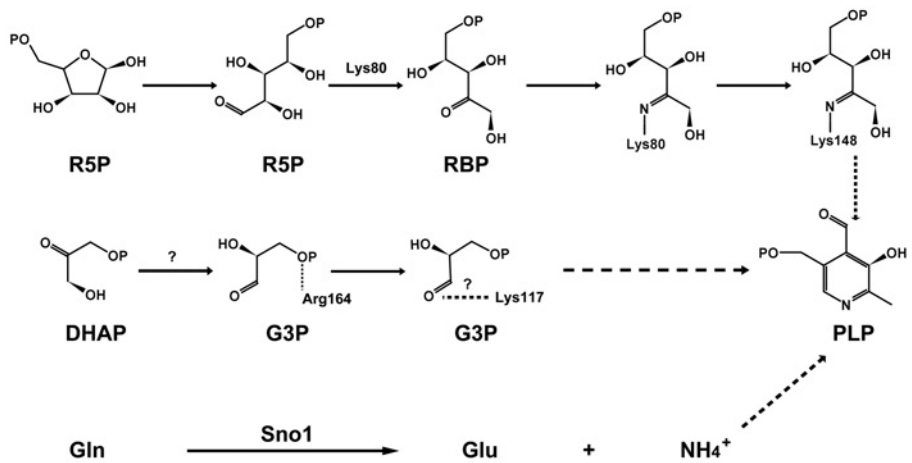

Scheme 2 Proposed catalytic mechanism for Snz1

in Snz1) has been excluded as a DHAP-isomerization site in a previous study [7]. The K117A and K148A mutants completely abolished PLP-synthesis activity (Supplementary Figure S1), but retained the capacity to catalyse DHAP isomerization (Supplementary Figure S4), whereas the K240A mutant had the same PLP-synthesis activity as the wild-type, using DHAP and RBP as substrates (Supplementary Figure S1). Moreover, the single-mutant R164A and the double-mutant R136A/R137A retained the same DHAP-isomerization activity as the wild-type (Supplementary Figure S4). The failure to assign the DHAP-isomerization site indicated that Snz1/Pdx1 might adopt an isomerization mechanism distinct from that of TIM.

Putative catalytic mechanism of Snz1

In the DXP-independent pathway, PLP is ultimately synthesized from the substrates R5P and DHAP, with ammonia hydrolysed from glutamine. Therefore Pdx1 catalyses not only PLP formation, but also the isomerization of R5P to RBP, and DHAP to G3P. In addition to the previously identified RBP-isomerization site [7], we found an additional three sites, one for PLP-formation, one for G3P-binding and the last for G3P-transfer. The high structural similarity of *Tm*Pdx1 and Snz1 enabled us to superimpose the structures of *Tm*Pdx1–RBP, Snz1–G3P and Snz1–PLP, which clearly showed the relative locations of the two substrates and the product (Figure 3).

Lys^{82} in *Tm*Pdx1 (Lys^{80} in Snz1) is proposed to catalyse the formation of the RBP imine from R5P, with the imine transferred to the Lys^{150} in *Tm*Pdx1 (Lys^{148} in Snz1) by a transimination reaction [7]. However, the structure of Snz1–PLP enabled us to assign Lys^{148} as the PLP-binding site, in addition to being an RBP imine acceptor. The Nε of Lys^{148} is 12.3 Å away from that of Lys^{80} in Snz1–PLP (Figure 3). The high *B*-factor of the loop from Lys^{148} to Thr^{153} indicated that it might undergo a conformational change, perhaps in combination with a side-chain rotation of Lys^{148}, to make Lys^{148} accessible to RBP for the transimination reaction.

Based on the G3P-binding site Arg$^{164'}$ and the transfer site Lys^{117}, we hypothesized that G3P (or G3P isomerized from DHAP) first binds to Arg$^{164'}$ of the neighbouring monomer and is transferred to Lys^{117}. The Nε of Lys^{117} is approx. 10.8 Å away from Nη1 of Arg$^{164'}$ and 10.7 Å from Nε of Lys^{148} (Figure 3), and is therefore in a relatively rigid loop of low *B*-factor. We propose

that G3P might be transferred from $Arg^{164'}$ to Lys^{117} via diffusion across the highly conserved interface. This unidirectional transfer route of G3P also explained why Snz1 catalyses the irreversible isomerization of DHAP to G3P.

On the basis of these findings, we propose the following catalytic mechanism for Snz1 (Scheme 2). R5P is isomerized to RBP, which forms an imine with Lys^{80} at the pentose isomerization site and is transferred to the PLP-formation site by a transimination reaction. Meanwhile, G3P or G3P isomerized from DHAP binds at the interface of the two Snz1 monomers (interacting with Arg^{164}, from the neighbouring monomer), before diffusion to Lys^{117}, which forwards it to the PLP-formation site (composed of Lys^{148}, Arg^{136} and Arg^{137}), where the third substrate, ammonia, is combined to form PLP.

AUTHOR CONTRIBUTION

Xuan Zhang carried out the site-directed mutagenesis, protein purification, crystallization and PLP synthesis assays, and wrote the paper. Yan-Bin Teng and Yong-Xing He performed the data collection and structure determination. Jian-Ping Liu and Xuan Zhang performed the DHAP/G3P isomerization assays. Kang Zhou contributed to the protein purification. Cong-Zhao Zhou and Yuxing Chen oversaw the project and wrote the paper.

ACKNOWLEDGEMENTS

We thank the staff at the Shanghai Synchrotron Radiation Facility for the help with data collection.

FUNDING

This work was supported by the National Natural Science Foundation of China [grant number 30870490]; and the Ministry of Science and Technology of China [grant numbers 2006CB910202, 2006CB806501].

REFERENCES

1 John, R. A. (1995) Pyridoxal phosphate-dependent enzymes. Biochim. Biophys. Acta **1248**, 81–96
2 Percudani, R. and Peracchi, A. (2003) A genomic overview of pyridoxal-phosphate-dependent enzymes. EMBO Rep. **4**, 850–854
3 Laber, B., Maurer, W., Scharf, S., Stepusin, K. and Schmidt, F. S. (1999) Vitamin B6 biosynthesis: formation of pyridoxine 5'-phosphate from 4-(phosphohydroxy)-L-threonine and 1-deoxy-D-xylulose-5-phosphate by PdxA and PdxJ protein. FEBS Lett. **449**, 45–48
4 Ehrenshaft, M., Bilski, P., Li, M. Y., Chignell, C. F. and Daub, M. E. (1999) A highly conserved sequence is a novel gene involved in de novo vitamin B6 biosynthesis. Proc. Natl. Acad. Sci. U.S.A. **96**, 9374–9378
5 Zhu, J., Burgner, J. W., Harms, E., Belitsky, B. R. and Smith, J. L. (2005) A new arrangement of $(\beta/\alpha)8$ barrels in the synthase subunit of PLP synthase. J. Biol. Chem. **280**, 27914–27923
6 Strohmeier, M., Raschle, T., Mazurkiewicz, J., Rippe, K., Sinning, I., Fitzpatrick, T. B. and Tews, I. (2006) Structure of a bacterial pyridoxal 5'-phosphate synthase complex. Proc. Natl. Acad. Sci. U.S.A. **103**, 19284–19289
7 Zein, F., Zhang, Y., Kang, Y. N., Burns, K., Begley, T. P. and Ealick, S. E. (2006) Structural insights into the mechanism of the PLP synthase holoenzyme from *Thermotoga maritima*. Biochemistry **45**, 14609–14620
8 Burns, K. E., Xiang, Y., Kinsland, C. L., McLafferty, F. W. and Begley, T. P. (2005) Reconstitution and biochemical characterization of a new pyridoxal-5'-phosphate biosynthetic pathway. J. Am. Chem. Soc. **127**, 3682–3683
9 Neuwirth, M., Strohmeier, M., Windeisen, V., Wallner, S., Deller, S., Rippe, K., Sinning, I., Macheroux, P. and Tews, I. (2009) X-ray crystal structure of *Saccharomyces cerevisiae* Pdx1 provides insights into the oligomeric nature of PLP synthases. FEBS Lett. **583**, 2179–2186
10 Dong, Y. X., Sueda, S., Nikawa, J. I. and Kondo, H. (2004) Characterization of the products of the genes SNO1 and SNZ1 involved in pyridoxine synthesis in *Saccharomyces cerevisiae*. Eur. J. Biochem. **271**, 745–752
11 Rodriguez-Navarro, S., Llorente, B., Rodriguez-Manzaneque, M. T., Ramne, A., Uber, G., Marchesan, D., Dujon, B., Herrero, E., Sunnerhagen, P. and Perez-Ortin, J. E. (2002) Functional analysis of yeast gene families involved in metabolism of vitamins B1 and B6. Yeast **19**, 1261–1276
12 McCoy, A. J. (2007) Solving structures of protein complexes by molecular replacement with Phaser. Acta Crystallogr. D Biol. Crystallogr. **63**, 32–41
13 Collaborative Computational Project No. 4 (1994) The CCP4 suite: programs for protein crystallography. Acta Crystallogr. D Biol. Crystallogr. **50**, 760–763
14 Murshudov, G. N., Vagin, A. A. and Dodson, E. J. (1997) Refinement of macromolecular structures by the maximum-likelihood method. Acta Crystallogr. D Biol. Crystallogr. **53**, 240–255
15 Emsley, P. and Cowtan, K. (2004) Coot: model-building tools for molecular graphics. Acta Crystallogr. D Biol. Crystallogr. **60**, 2126–2132
16 Lovell, S. C., Davis, I. W., Arendall, 3rd, W. B., de Bakker, P. I., Word, J. M., Prisant, M. G., Richardson, J. S. and Richardson, D. C. (2003) Structure validation by Cα geometry: φ, ψ and Cβ deviation. Proteins **50**, 437–450
17 Raschle, T., Amrhein, N. and Fitzpatrick, T. B. (2005) On the two components of pyridoxal 5′-phosphate synthase from *Bacillus subtilis*. J. Biol. Chem **280**, 32291–32300
18 O'Donoghue, A. C., Amyes, T. L. and Richard, J. P. (2005) Hydron transfer catalyzed by triosephosphate isomerase products of isomerization of dihydroxyacetone phosphate in D_2O. Biochemistry **44**, 2622–2631
19 O'Donoghue, A. C., Amyes, T. L. and Richard, J. P. (2005) Hydron transfer catalyzed by triosephosphate isomerase products of isomerization of (R)-glyceraldehyde 3-phosphate in D_2O. Biochemistry **44**, 2610–2621
20 Holm, L. and Sander, C. (1993) Protein structure comparison by alignment of distance matrices. J. Mol. Biol. **233**, 123–138
21 Noble, M. E., Wierenga, R. K., Lambeir, A. M., Opperdoes, F. R., Thunnissen, A. M., Kalk, K. H., Groendijk, H. and Hol, W. G. (1991) The adaptability of the active site of trypanosomal triosephosphate isomerase as observed in the crystal structures of three different complexes. Proteins **10**, 50–69
22 Lolis, E., Alber, T., Davenport, R. C., Rose, D., Hartman, F. C. and Petsko, G. A. (1990) Structure of yeast triosephosphate isomerase at 1.9-Å resolution. Biochemistry **29**, 6609–6618
23 Schliebs, W., Thanki, N., Eritja, R. and Wierenga, R. (1996) Active site properties of monomeric triosephosphate isomerase (monoTIM) as deduced from mutational and structural studies. Protein Sci. **5**, 229–239
24 Lodi, P. J., Chang, L. C., Knowles, J. R. and Komives, E. A. (1994) Triosephosphate isomerase requires a positively charged active site: the role of lysine-12. Biochemistry **33**, 2809–2814

Received 10 August 2010/20 September 2010; accepted 5 October 2010
Published as BJ Immediate Publication 5 October 2010, doi:10.1042/BJ20101241

online data

SUPPLEMENTARY ONLINE DATA

Structural insights into the catalytic mechanism of the yeast pyridoxal 5-phosphate synthase Snz1

Xuan ZHANG, Yan-Bin TENG, Jian-Ping LIU, Yong-Xing HE, Kang ZHOU, Yuxing CHEN and Cong-Zhao ZHOU[1]

Hefei National Laboratory for Physical Sciences at Microscale and School of Life Sciences, University of Science and Technology of China, Hefei, Anhui 230027, People's Republic of China

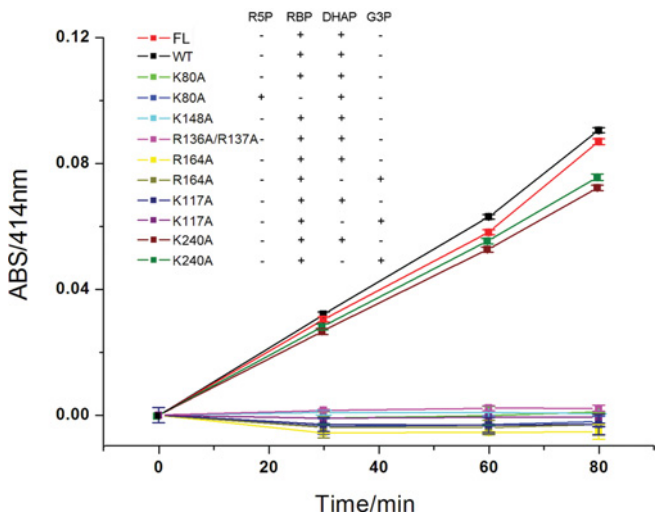

Figure S1 The relative activity of Snz1 and mutants

FL, full-length; WT, wild-type.

EXPERIMENTAL

Cloning and expression

The coding region of the *SNZ1* gene was amplified by PCR using *Saccharomyces cerevisiae* S288C genomic DNA as a template. The PCR product was cloned into a pET28 expression vector (Novagen) downstream of a His_6 tag between NdeI and NotI restriction sites. The NdeI/NotI restriction fragment of the PCR product was purified and cloned into the pET28 expression vector (Novagen). K80A, E116A, K117A, R136A/R137A, K148A, R164A and K240A were generated via PCR-based site-directed mutagenesis. The proposed residues were substituted by using the mutagenic primers that have been designed according to the 5′- and 3′-sequence of the Snz1 wild-type gene. These corresponding overexpression plasmids were transformed into competent *E. coli* Bl21 (DE3) (Novagen) cells and the transformed cells were grown at 37°C in 2×YT medium to an D_{600nm} of 0.6–0.8. Expression of Snz1 was induced by adding IPTG (isopropyl β-D-thiogalactopyranoside) to a final concentration of 0.2 mM, and then the cells were allowed to grow for a further 4 h. After that, the cells were harvested by centrifugation (8000 ***g*** for 8 min at 4 °C) and the pellet was resuspended in 10 ml of 20 mM Tris/HCl (pH 8.0) and 200 mM NaCl.

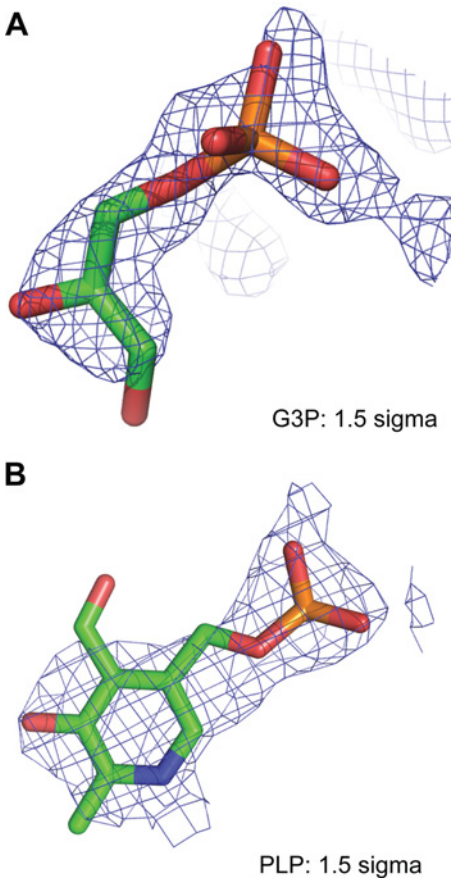

Figure S2 The electron density map of (A) G3P and (B) PLP, at 1.5 σ

Purification and crystallization

The cells were disrupted by sonication (5 cycles, 30 s per cycle, 1:1 pulse/pause at 50 % amplitude of 750 W) and then centrifuged for 30 min at 16 000 ***g*** at 4°C. After that, the supernatant was loaded on to a 1 ml HiTrap chelating HP column (GE healthcare) and eluted with imidazole gradient. Eluted protein was further purified by gel filtration using a HiLoad 16/60 Superdex 200 column (Amersham Biosciences) equilibrated with buffer containing 20 mM Tris/HCl (pH 8.0) and 200 mM NaCl (for crystallization), or 50 mM Tris/HCl (pH 8.0) (for enzymatic assays). The protein was dialysed against 20 mM Tris/HCl (pH 8.0) and 20 mM NaCl, and concentrated to approx. 10 mg/ml prior to crystal screening. The protein Snz1 was co-crystallized respectively with 2.5 mM PLP or 10 mM DHAP at 16°C using the hanging drop vapour

[1] To whom correspondence should be addressed (email zcz@ustc.edu.cn).

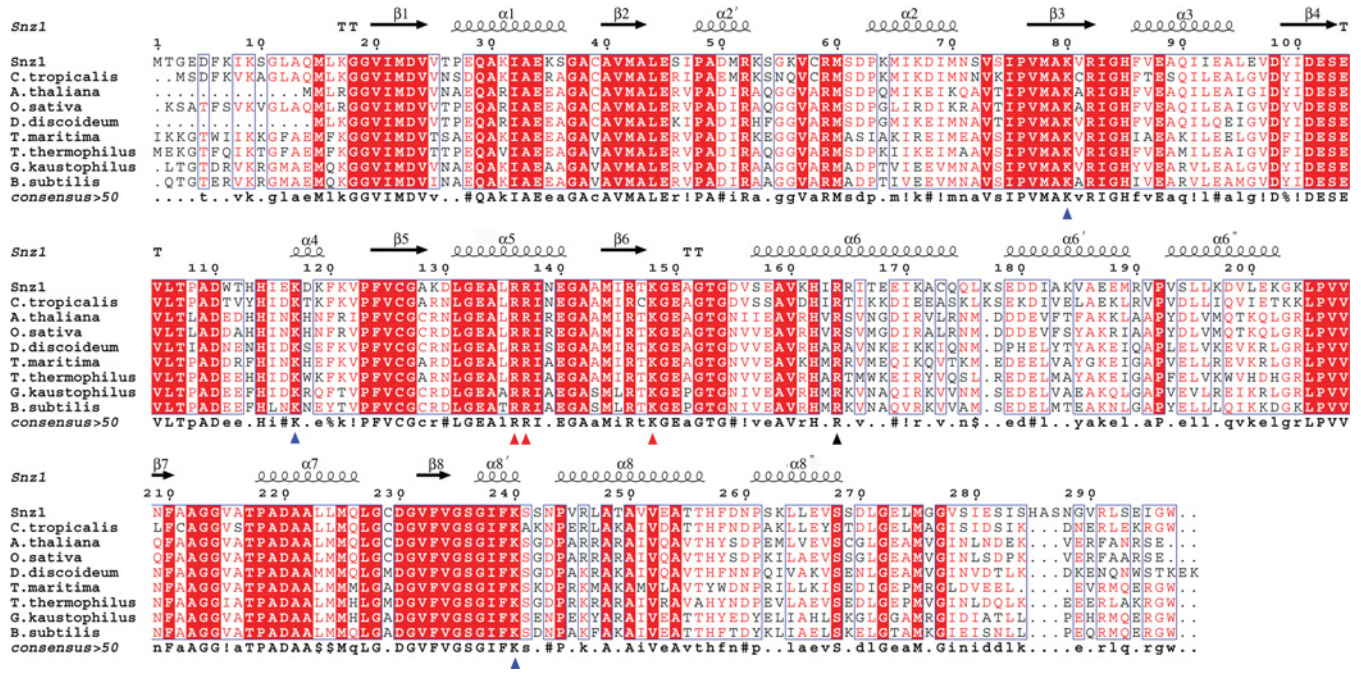

Figure S3 Multi-alignment of Snz1 against PLP synthases from *Candida tropicalis* (XP_002550328.1), *Arabidopsis thaliana* (NP_195761.1), *Oryza sativa* (NP_001058669.1), *Dictyostelium discoideum* (XP_636800.1), *Thermotoga maritima* (NP_228283.1), *Thermus thermophilus* (YP_143970.1), *Geobacillus kaustophilus* (YP_145864.1) and *Bacillus subtilis* (NP_387892.1)

G3P-binding sites are indicated with black arrows, PLP is indicated with red arrows and conserved lysine residues are indicated with blue arrows. All sequences were from NCBI databases. Multi-alignment was performed with the programs MultAlin [1] and ESPript [2].

diffusion method from a 1:1 mixture of protein and well solution. The reservoir solution for the optimized conditions contained 20 % PEG [poly(ethylene) glycol] 400, 0.1 M $MgCl_2$ and 0.1 M Hepes (pH 7.5). Twin-crystals appeared in 2 days, and then were washed in well solution, crushed and diluted for microseeding (1 μl) into drops containing 5 μl of protein solution and 4 μl of well solution. The crystals grew over 5 days to their maximum size (approx. 0.3 mm×0.3 mm×0.2 mm). Both the crystals of apo-form, Snz1–PLP and Snz1–G3P are in space group $P22_12_1$ with three polypeptides in the asymmetric unit.

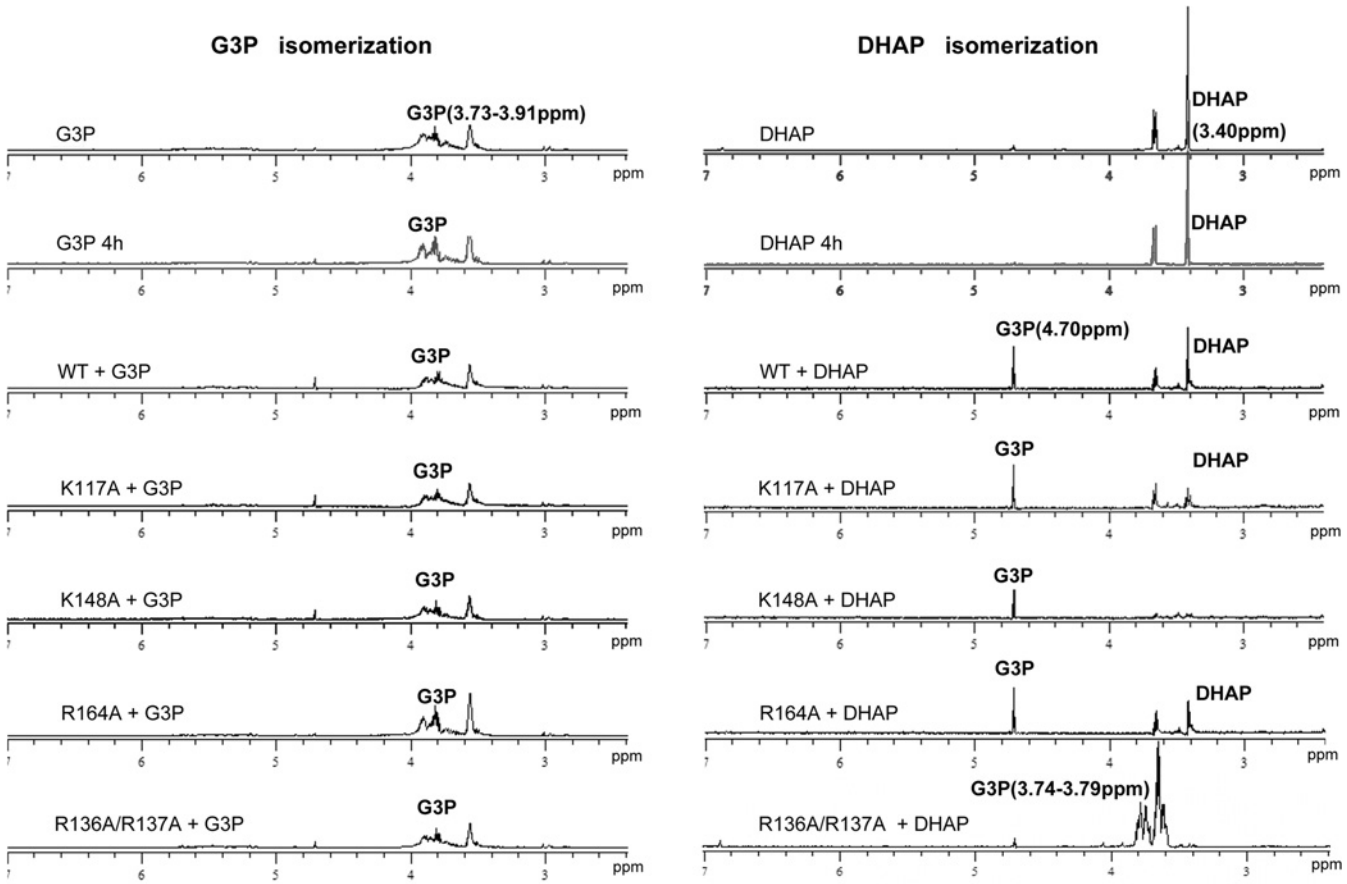

Figure S4 TIM activity of Snz1 and mutants

Representative partial ^{1}H-NMR spectra of the remaining substrate and the products during the reaction of G3P (10 mM) or DHAP (10 mM) catalysed by Snz1 and mutants (40 μM) in $^{2}H_2O$ buffered by 50 mM phosphate, pD 8.0.

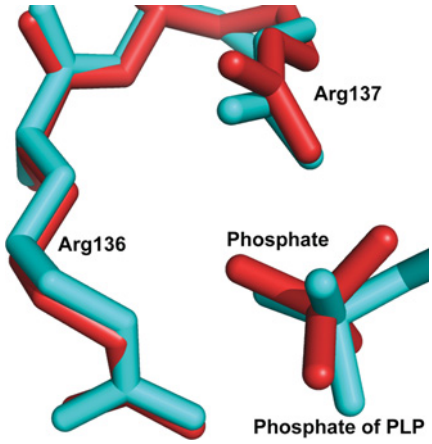

Figure S5 Superposition of phosphate ion (red) in *Tm*YaaD and PLP phosphate group (cyan) in Snz1

Received 10 August 2010/20 September 2010; accepted 5 October 2010
Published as BJ Immediate Publication 5 October 2010, doi:10.1042/BJ20101241

REFERENCES

1 Corpet, F. (1988) Multiple sequence alignment with hierarchical clustering. Nucleic Acids Res. **16**, 10881–10890
2 Gouet, P., Robert, X. and Courcelle, E. (2003) ESPript/ENDscript: extracting and rendering sequence and 3D information from atomic structures of proteins. Nucleic Acids Res. **31**, 3320–3323